Low-Cost and High-Performance 5-Bit Programmable Phased Array at Ku-Band

**Xin Li[1], Han Qing Yang[1], Rui Wen Shao[1], Feng Zhai[1],
Guo Biao Liu[1], Zheng Xing Wang[1], Hong Fei Gao[1], Ge Fan[1],
Jun Wei Wu[1, 2, 3, *], Qiang Cheng[1, 2, 3, *], and Tie Jun Cui[1, 2, 3, *]**

Abstract—We present a low-cost and high-performance 5-bit programmable phased array antenna at Ku-band, which consists of 1-bit reconfigurable radiation structures, digital phase shifters, and a coplanar waveguide feeding network. The 1-bit reconfigurable radiation structure utilizes symmetric geometries and PIN diodes to form stable 180° phase difference. The digital phase shifter provides 168.75° phase difference and together with the radiation structure form a 348.75° phase coverage. The antenna operates between 14.4 and 15.4 GHz, and the overall array contains 24 × 2 elements with each of them being individually addressable. By changing the states of the diodes and thus adjusting the phase coding sequences of the array, the antenna achieves 0°–60° precise beam scanning at 14.8 GHz, with the sidelobe level, cross-polarization, and gain fluctuation being less than −16 dB, −26 dB, and 2.4 dB, respectively. A prototype was fabricated to verify the design, and the measurement results agree well with simulations. Compared with traditional phased arrays composed of numerous phase shifters and T/R components, the proposed antenna features high performance, high flexibility, low profile, and low cost. The antenna provides a new and feasible solution of wavefront steering and will benefit the various application scenarios.

1. INTRODUCTION

Over the past decades, phased array antennas have been widely used in various wireless applications including radar tracking, remote sensing, and satellite communication because of their fast and accurate beam scanning capabilities [1–4]. However, a large number of electronic phase shifters or T/R components are required in traditional phased arrays, which undoubtedly brings high cost, high power consumption, and large profile. Reconfigurable array antennas have the advantages of being compact, light weight, cheap, and can be easily integrated with other components [5–7]. In particular, pattern reconfigurable antennas have exhibited powerful capabilities in real-time beam steering and played important roles in various scenarios [8–10]. Therefore, they serve as predominant alternatives to traditional phased arrays.

Pattern reconfigurability is usually realized by using two methods. The first method is to change the radiation patterns of the constituent array elements. For example, in [11] the beam directions of patch antennas were controlled by changing the on-off state of the PIN diodes loaded on three parallel coupling slots, and then the overall pattern of the proposed 1×4 array pointed to five different directions. In [12], the radiation mode of the Yagi antenna element was altered by tuning the four loaded varactor

diodes, and the array realized wide-angle beam scanning. [13] proposed a patch antenna with four reconfigurable beams in the azimuth plane by switching over different sets of feeding ports.

The second method is to adjust the phase distributions of array elements. Different from conventional phased arrays that utilize phase-shifting networks, the so called digital bit arrays achieve phase shifting by changing the states of the embedded components including PIN diodes [14], varactor diodes [15], liquid crystals [16], graphene [17], etc. The recently proposed reconfigurable reflectarrays (RRAs) and transmitarrays (RTAs) are examples of this class [18–21]. However, they have large profiles due to the restrictions of the feeding mechanism. Driven by the need for miniaturization, several self-feeding planar reconfigurable bit arrays were proposed. In [22], a 1-bit reconfigurable patch array antenna was achieved by exploiting structural symmetry. By changing the coding sequence, the antenna realized different radiation patterns such as sum-, dual-, and quad-beams. In addition, a circularly polarized 2-bit reconfigurable array antenna was implemented for single-beam scanning [23]. Furthermore, high sidelobe levels (SLLs) induced by 2-bit phase quantization were suppressed by rotating array elements randomly [5].

It is noted that limited number of pattern states in the first method imposes severe restriction on the realization of high-precision beam scanning. In comparison, the second method is superior in this respect. However, current studies on reconfigurable bit arrays only realize rough phase quantization, and the beam scanning performance is no doubt limited in terms of scanning precision and radiation efficiency. To the best of our knowledge, the current literature can achieve up to 2-bit phase quantization and step of $45°$. Therefore, reconfigurable bit arrays with high phase resolutions are highly desired yet still elusive.

In this paper, we propose a 24×2 element and 5-bit programmable phased array antenna operating in the Ku-band. The antenna is composed of 1-bit reconfigurable radiation structures, digital phase shifters, and a coplanar waveguide feeding network. The radiation structure provides $180°$ phase shift by changing the on-off states of two symmetrically loaded PIN diodes. A reflection-type phase shifter integrated with two varactor diodes provides $168.75°$ phase difference. In total, 5-bit phase quantization can be obtained with the coverage of $348.75°$ and step of $11.25°$. Compared with conventional phased arrays, the design does not need numerous electronic phase shifters or T/R components, thus significantly reducing the profile, complexity, and costs. An antenna prototype with 24×2 individually addressable elements was fabricated and measured to validate the novel design. The simulated and measured results show that the design achieves high-precision and large-angle beam scanning with low gain fluctuation, low SLL, and low cross-polarization. The novel design provides a new and feasible solution of wavefront steering and will benefit the various application scenarios.

2. DESIGN AND ANALYSIS OF THE 1-BIT RECONFIGURABLE ANTENNA AND 4-BIT DIGITAL PHASE SHIFTER

2.1. 1-Bit Antenna Configuration and Performance Analysis

The configuration of the 1-bit reconfigurable antenna is presented in Figure 1, which contains two dielectric substrates and three metallic layers. As shown in Figure 1(a), a slotted patch is located on the top layer, while the ground plane and the switchable feeding structure are located on the middle and bottom layers, respectively. The substrates are Rogers 4003C laminates ($\varepsilon r = 3.55$ and $\tan \delta = 0.0027$ at $10\,\text{GHz}$), and the top and bottom layers are bonded together by the prepreg Rogers 4450F ($\varepsilon r = 3.7$ and $\tan \delta = 0.004$ at $10\,\text{GHz}$). The dimensions of the radiation structure are shown in Table 1.

Table 1. Dimensions of the 1-bit antenna (unit: mm).

L	h_1	h_2	h_b	pl	pw	sl	sw	df	wm
10	1.524	0.203	0.1	5	5	4.75	1.5	2.7	0.68

The proposed antenna utilizes structural symmetry to achieve 1-bit phase modulation. As shown in Figures 1(a) and 1(b), the two feeding probes are symmetrically connected with the slotted patch of the antenna. When the signal is given to the slotted patch from the left and right feeding probes,
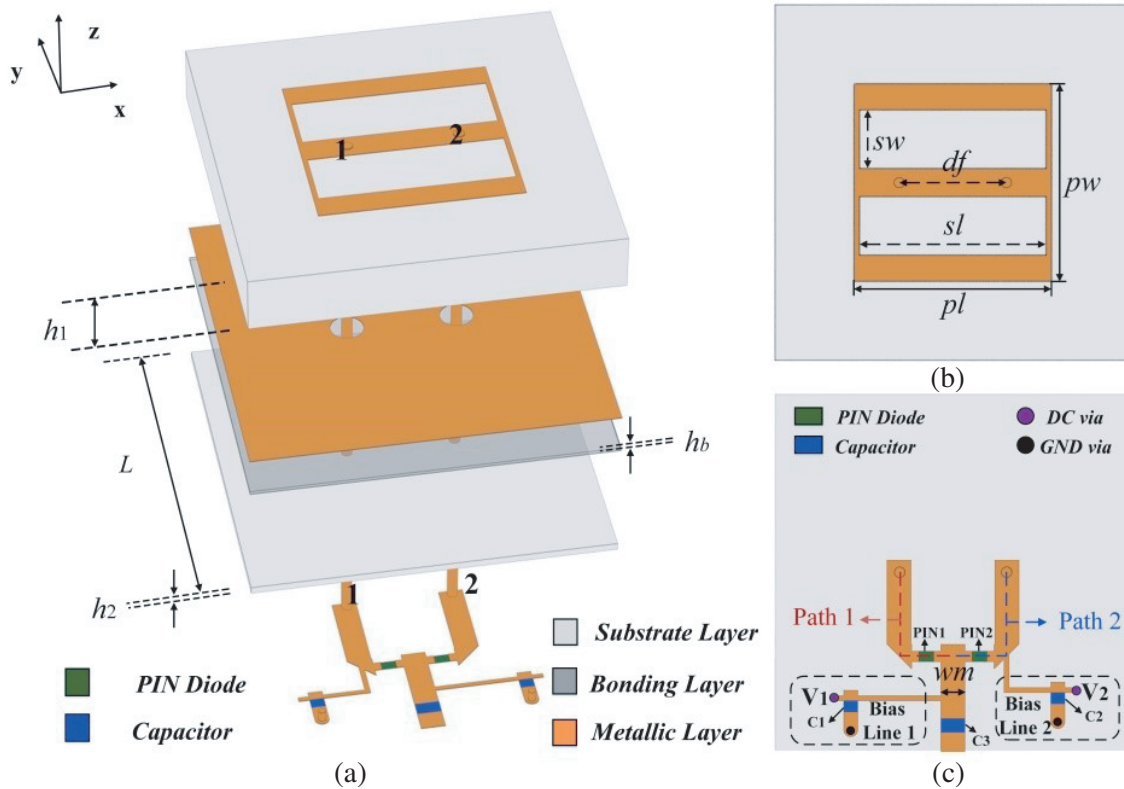
Figure 1. Configuration of the proposed 1-bit reconfigurable antenna. (a) Exploded view. (b) Top view. (c) Bottom view.

respectively, two surface currents with the same amplitudes but opposite phases are naturally excited. Here, we say that the antenna is in the "0" state when it is fed by the left probe and in the "1" state when it is fed by the right probe. The switching is realized by changing the on-off states of PIN1 and PIN2 (MADP-14020-907) in the structure given by Figure 1(c). For the on state, the PIN diode is modeled as a series of 7.8-Ω lumped resistance and 30-pH inductance. For the off state, the PIN diode is modeled as a series of 0.025-pF capacitance and 30-pH inductance.

Since slotted patches are superior to rectangular patches in increasing the impedance bandwidth and suppressing cross-polarization, we chose the configuration in Figure 1(b) as the basic radiation structure, for the analysis, refer to the appendix. The biasing circuit is important for efficient switch of the states of the PIN diodes. In Figure 1(c), we can see that the designed biasing circuit consists of biasing lines, capacitors, DC vias, and GND vias. The DC signal enters the circuit through two DC vias and only needs to adjust the voltage values of V_1 and V_2 to control the state of the diodes. The biasing lines have a width of 0.1 mm with high impedance. The grounded capacitors C1 and C2 filter the AC signal from the DC signal. The capacitor C3 on the signal input path is used to isolate the DC signal from the AC. All the three capacitors are 0.5 pF. The working states of the whole structure are summarized in Table 2.

Table 2. Reconfigurable states of the 1-bit antenna.

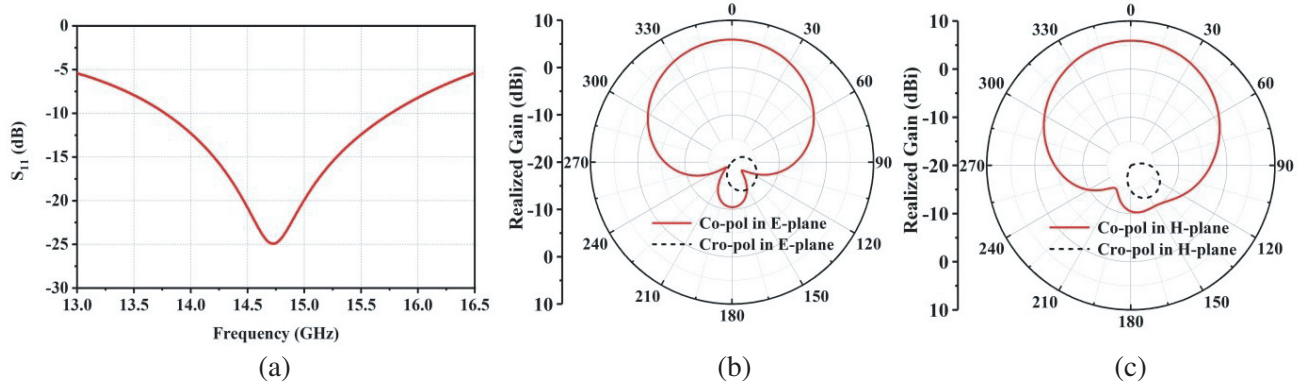| Antenna State	PIN 1	PIN 2	Feeding Probe	Phase State	V_1 (V)	V_2 (V)
0	On	Off	1	0°	1.5	1.5
1	Off	On	2	180°	3	0

Figure 2. (a) Simulated reflection coefficients (S_{11}) of the proposed antenna; (b) Simulated radiation patterns of the proposed antenna at 14.8 GHz in the E-plane; (c) Simulated radiation patterns of the proposed antenna at 14.8 GHz in the H-plane.

On the basis of the above analysis, a high-performance 1-bit reconfigurable antenna is realized. We employ the commercial software, CST MICROWAVE STUDIO to simulate the proposed antenna [24]. The operating frequency ($|S_{11}| < -10$ dB) is from 13.7 to 15.7 GHz, as shown in Figure 2(a). The radiation patterns are illustrated in Figures 2(b) and 2(c). The gain of co-polarization at 14.8 GHz is 5.9 dBi, with a half-power beamwidth of 86.2° in the E-plane and 90.3° in the H-plane. The cross-polarization is -26.3 dB in the broadside direction. It is worth mentioning that the patterns of the antenna working in the "0"/"1" states are basically the same because of the symmetry of the structure.

Figure 3(a) shows the surface current distributions of the proposed antenna in the "0" and "1" states at 14.8 GHz. It can be observed that the two groups of currents have the same amplitudes but opposite phases. Additionally, the phases of the corresponding electric fields (obtained by an electric field probe in the far-field region) shown in Figure 3(b) have stable 180° phase difference over the bandwidth. As a result, a 1-bit phase quantization is obtained.
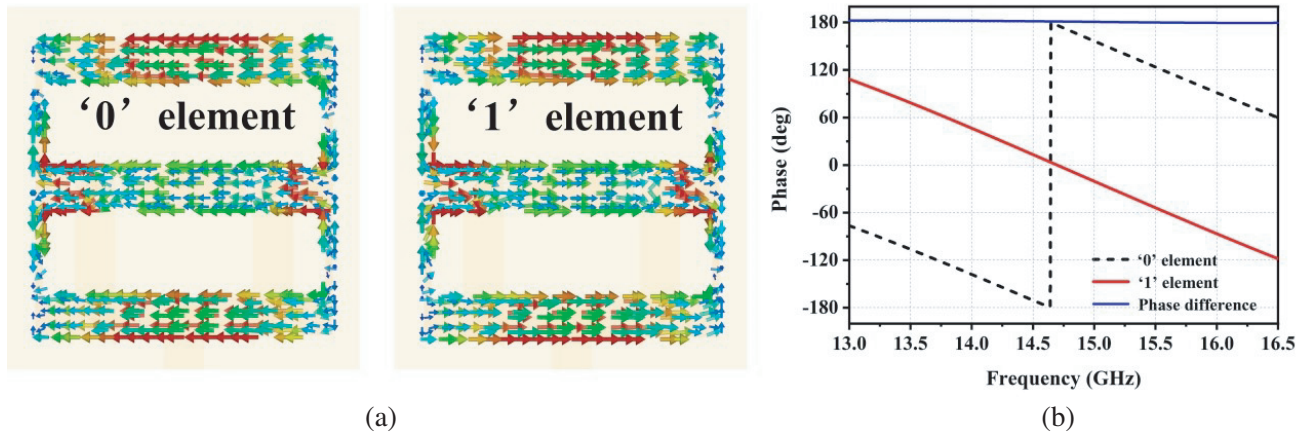

Figure 3. (a) Surface current distribution of the proposed antenna in the "0" and "1" states at 14.8 GHz. (b) The electric field phases and the corresponding phase difference in the "0" and "1" states.

2.2. Analysis and Design of the 4-Bit Digital Phase Shifter

Up to now, we have designed a 1-bit reconfigurable antenna and obtained stable 180° phase shift without using phase shifters. In order to improve the scanning capability and pattern performance of the phased array, we further design the digital reflection-type phase shifter illustrated in Figure 4, thus extending
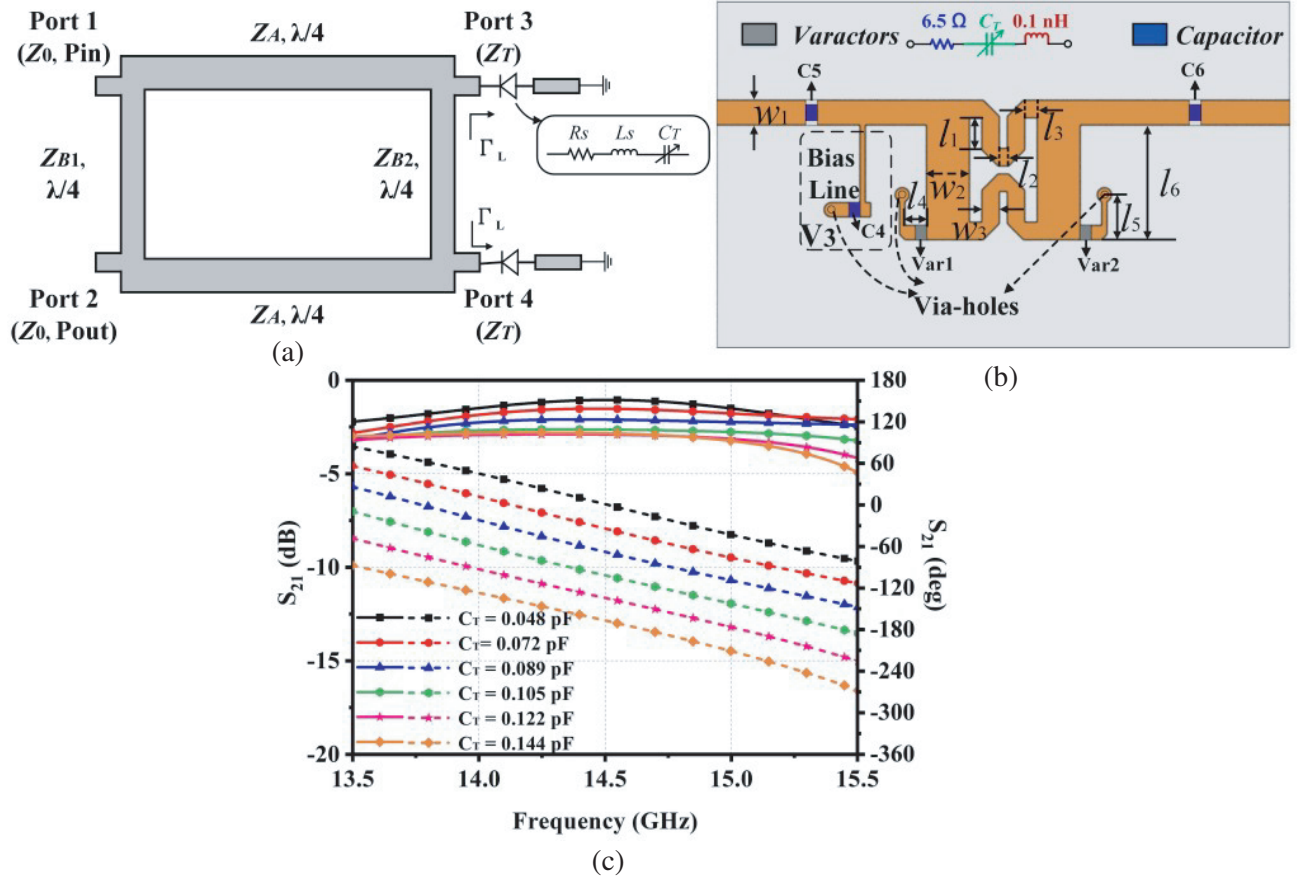
Figure 4. (a) Schematic of the proposed digital reflection-type phase shifter. (b) Geometry of the phase shifter. Detailed dimensions: $w_1 = 0.69\,\text{mm}$, $w_2 = 1.2\,\text{mm}$, $w_3 = 0.5\,\text{mm}$, $l_1 = 0.89\,\text{mm}$, $l_2 = 0.2\,\text{mm}$, $l_3 = 0.35\,\text{mm}$, $l_4 = 0.6\,\text{mm}$, $l_5 = 1.25\,\text{mm}$, and $l_6 = 3.2\,\text{mm}$. (c) Simulated transmission coefficients (S_{21}) of the 4-bit digital phase shifter.

the phase shifting capability of the 1-bit reconfigurable antenna. The schematic of the proposed digital reflection-type phase shifter is shown in Figure 4(a), which consists of a 3-dB impedance-transforming branch-line coupler and two terminated identical reflection loads [25, 26]. By adjusting the impedance of the reflected loads, one can induce a relative phase shift between the input and output ports of the reflection-type phase shifter [27]. The load is composed of a varactor diode and a transmission line section. Introducing the transmission line section is equivalent to connecting an inductance to the varactor diode in series, thus extending the phase-shift range of the circuit [28]. For the 3-dB impedance-transforming branch-line coupler, the characteristic impedance of each branch is $Z_{B1} = Z_0$, $Z_{B2} = Z_0/r_Z$, $Z_A = Z_0/\sqrt{2r_Z}$, where r_Z is the impedance ratio [29]. For the reflection load, the port impedance Z_T is equal to the sum of the input impedance of the transmission line Z_{line} and varactor diode Z_{var}, where $Z_{line} = jZ_1 \tan \beta l$, $Z_{var} = R_S + j\omega L_S + 1/j\omega C_T$.

According to the transmission-line theory, the reflection coefficient of one reflection load can be obtained as [30]

$$\Gamma_L = |\Gamma_L| e^{j\varphi_{21}} = \frac{Z_L - Z_0}{Z_L + Z_0} = \frac{Z_T - Z_{B2}}{Z_T + Z_{B2}} = \frac{(r_z R_S - Z_0) + jr_z X_L}{(r_z R_S + Z_0) + jr_z X_L}. \tag{1}$$

where X_L is equal to $Z_1 \tan \beta l + \omega L_S - 1/\omega C_T$.

Therefore, the relative phase shift φ between input and output ports caused by the reflection load

can be expressed as [27]

$$\varphi = \frac{\pi}{2} + \varphi_{21} = \frac{\pi}{2} + \tan^{-1}\frac{r_z X_L}{r_z R_S - Z_0} - \tan^{-1}\frac{r_z X_L}{r_z R_S + Z_0}. \tag{2}$$

The phase difference $\Delta\varphi$ resulting from the relative phase shift between the maximum and minimum values of the varactor capacitance is

$$\Delta\varphi = |\varphi_{\max} - \varphi_{\min}| = |\varphi_{21}(X_{L,\max}) - \varphi_{21}(X_{L,\min})|. \tag{3}$$

where $X_{L,\max} = Z_1 \tan\beta l + \omega L_S - 1/\omega C_{T,\max}$, $X_{L,\min} = Z_1 \tan\beta l + \omega L_S - 1/\omega C_{T,\min}$.

Based on the results of the above theoretical analysis, a digital reflection-type phase shifter operating at Ku-band is designed as shown in Figure 4(b). The substrate is laminated Rogers 4003C with thicknesses of $0.203\,\text{mm}$. And the geometrical parameters in the figure are given in the underlying caption. A bent microstrip line is used in the branch-line coupler, whose size is $4.24 \times 4.1\,\text{mm}^2$, about 33% of the simple design that use straight quarter-wavelength line. The two terminals of the coupler are connected with tunable reflection loads composed of varactor diodes (MAVR-011020-1411, whose equivalent circuit is shown in the top of Figure 4(b)) and transmission line sections. A circuit with isolation effect is designed to bias the varactor diodes and at the same time reduce the interaction between AC and DC signals. The DC bias line is composed of the grounded capacitor C4 and the quarter-wavelength-high impedance line, which isolates AC signals. The two capacitors (C5 and C6) connected in series with the input and output ports of the phase shifter isolate the DC signal. The capacitors herein are all $100\,\text{pF}$.

The input and output ports of the whole digital phase shifter are symmetrically matched to $50\,\Omega$. The size of the 3-dB impedance-transforming branch-line coupler and the length of the series transmission line in the reflection loads are optimized. The capacitance value of the varactor diode can be continuously adjusted by the voltage V_3, and a continuous phase change can then be obtained. Here, we limit the phase control range to $168.75°$ and perform 4-bit phase quantization, which shows a good trade-off between the subsequent control circuit design and insertion loss. Table 3 lists the corresponding relationship between the control voltage V_3 and the capacitance value C_T of the varactor and the phase shift. When the capacitance changes from 0.048 to $0.144\,\text{pF}$, the corresponding transmission amplitude and phase of the phase shifter are shown in Figure 4(c). Within the desired band centered at $14.8\,\text{GHz}$, the relative phase shift can be stabilized at 4-bit ($168.75°$), and the insertion losses of all states are below $-3\,\text{dB}$.

Table 3. Corresponding relationship between control voltage V_3 and the capacitance value C_T of the varator and the phase shifter.

V_3 (V)	C_T (pF)	PS (°)	V_3 (V)	C_T (pF)	PS (°)	V_3 (V)	C_T (pF)	PS (°)	V_3 (V)	C_T (pF)	PS (°)
1.21	0.144	0	1.46	0.137	11.25	1.69	0.129	22.5	1.91	0.122	33.75
2.15	0.116	45	2.38	0.110	56.25	2.64	0.105	67.5	2.92	0.100	78.75
3.23	0.094	90	3.59	0.089	101.25	4.01	0.083	112.5	4.53	0.078	123.75
5.19	0.072	135	6.12	0.065	146.25	7.5	0.058	157.5	9.7	0.048	168.75

3. 5-BIT PROGRAMMABLE PHASED ARRAY ANTENNA

By cascading the 1-bit antenna that has $180°$ relative phase shift and phase shifter that has $168.75°$ relative phase shift, we can obtain a 5-bit antenna with a $348.75°$ relative phase shift. Compared with conventional phased array antennas that generate phase states by cascading multiple phase shifters, the 5-bit antenna here can reduce both the path insertion loss and geometry size. Following this strategy, we design the 24×2 programmable phased array antenna depicted in Figure 5. The antenna can be regarded as a linear array in the H-plane. Two array elements are arranged in parallel as a branch in the E-plane to improve the array gain. The intervals between adjacent array elements in E-plane and
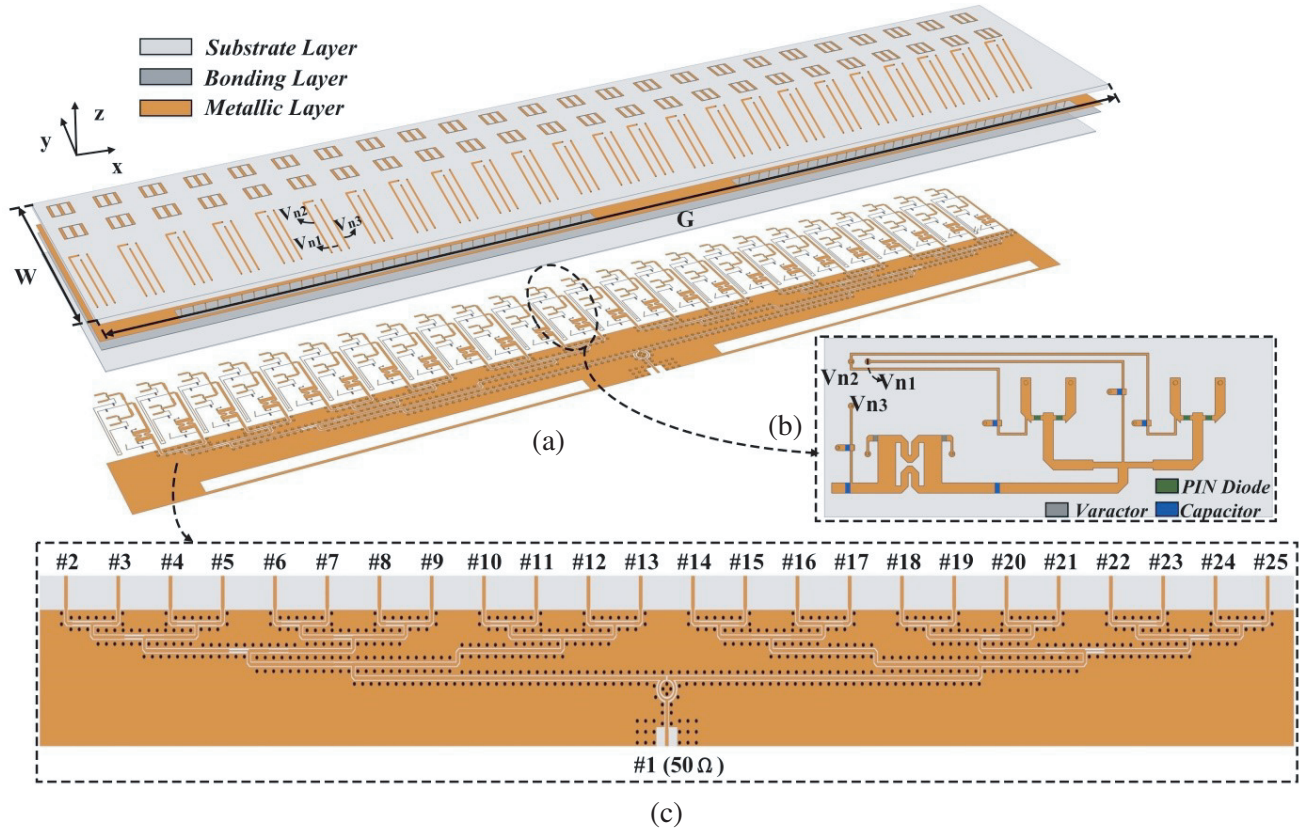
Figure 5. Configuration of the 24×2 5-bit programmable phased array antenna.

H-plane are 10 mm, about $0.5\lambda_0$ (λ_0 is the free space wavelength at 14.8 GHz). The overall size of the antenna is $G \times W = 250 \times 50 \, \text{mm}^2$. The interlayer structure of the whole antenna is consistent with the 1-bit radiation structure, and the thickness is only 1.881 mm, about $0.09\lambda_0$ at 14.8 GHz. A $1 : 24$ coplanar waveguide with ground (CPWG) network feeds the array elements as shown in Figure 5(c). The simulated currents on the feeding network at 14.4, 14.8, and 15.4 GHz are plotted in Figure 6,
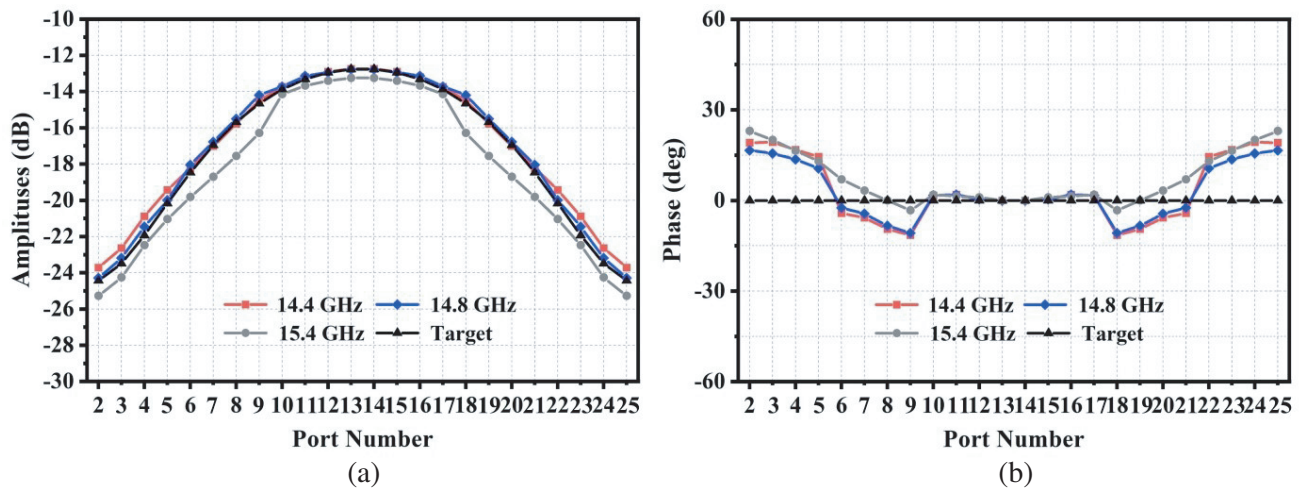

Figure 6. Targeted and simulated amplitude and phased distributions of the 24-way Taylor CPWG feeding network at 14.4, 14.8, and 15.4 GHz.

which follow the Taylor distribution and help to reduce the SLL of the array pattern.

In order to demonstrate the beam scanning capability of the array, we next synthesize the array pattern according to the following equation

$$F(\theta) = \sum_{n=1}^{N} a_n(\theta) e^{j(k_0 d \sin \theta + \delta(n))}. \tag{4}$$

where $a_n(\theta)$ is the amplitude of the nth element, k_0 the wavenumber, and θ the angle of the pitch in a spherical coordinate, while d and $\delta(n)$ are the distance and phase difference between adjacent elements, respectively. For conventional phased arrays, the excitation phase difference can be written as

$$\Delta\varphi(n) = -k_0 d \sin \theta, \quad n = 1, 2, \ldots, N. \tag{5}$$

For the k-bit phased array, the excitation phase must be quantized. First, it is normalized to $(-180°, 180°)$ according to the following equation:

$$\psi_{\text{nor}}(n) = 360 \times \left| \frac{\Delta\varphi(n) \times (n-1)}{2\pi} \right| - 180. \tag{6}$$

The quantization step is $\Delta = 2\pi/2^k$. Therefore, the quantized phase of the nth k-bit array element can be expressed as

$$\psi_{\text{qua}}(n) = \left\lfloor \frac{\psi_{\text{nor}}(n)}{\Delta} + \frac{1}{2} \right\rfloor \times \Delta \quad (n = 1, 2, \ldots, N). \tag{7}$$

Using Equations (5)–(7), we compute the quantized phase distribution of the 5-bit programmable phased array versus representative scanning angles at 14.8 GHz, which is depicted in Figure 7(a). The phases therein can be realized by changing the voltages V_{n1} and V_{n2} on PIN diodes and the voltage V_{n3} on varactor diode, as drawn in Figure 5(b). The simulated S_{11} values of the phased array with different scanning angles are shown in Figure 7(b). The -10 dB impedance-matched frequency band is from 14.4 to 15.4 GHz. Moreover, the S_{11} values under different scanning angles are basically the same. The simulated scanning radiation patterns in the H-plane at 14.4, 14.8, and 15.4 GHz are shown in Figures 8(a)–8(c), respectively. We can find that the radiation beam is steered from $0°$ to $60°$ with a step of $10°$. The scanning coverages at the three frequency points are $0°$ to $61°$, $0°$ to $60°$, and $0°$ to $56°$, respectively. The direction of the array pattern at 14.8 GHz is very accurate, whereas there are small derivations at the low and high frequencies for a specific coding sequence caused by different wave numbers at different frequencies.

We investigate the pointing precision, array gain, SLL, and cross-polarization characteristics of the antenna, as shown in Figure 9, to further evaluate its scanning performance. The maximum realized
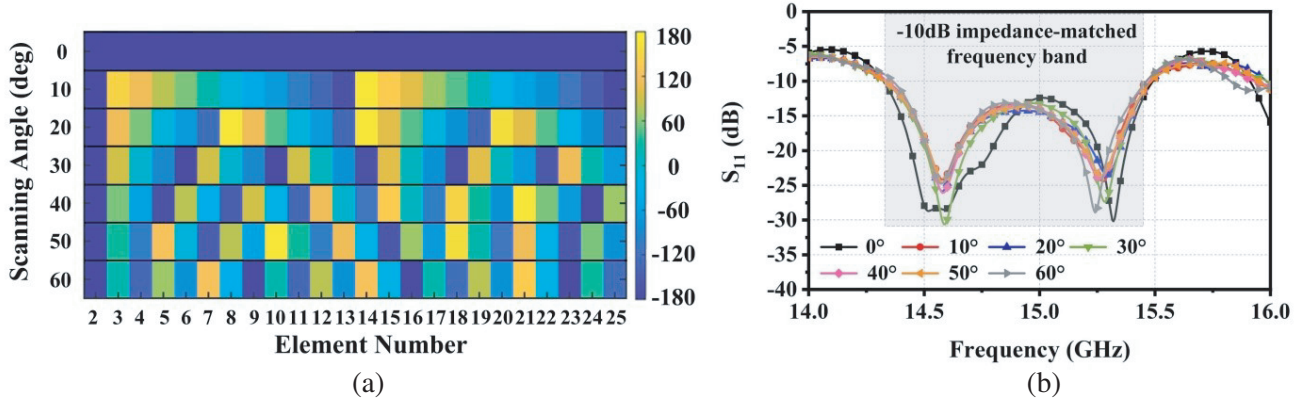

(a)   (b)

Figure 7. (a) Quantized excitation phase distribution of the 5-bit programmable phased array corresponding to some representative scanning angles at 14.8 GHz. (b) Simulated S_{11} of the proposed 5-bit programmable phased array with different scanning angles.
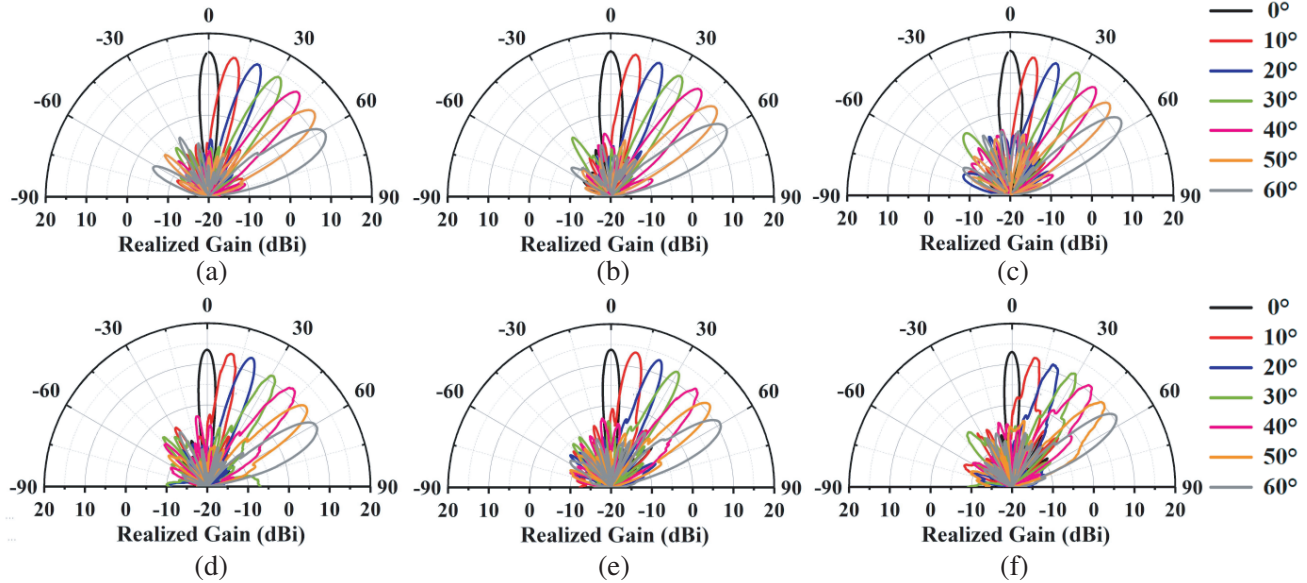
Figure 8. Simulated and measured radiation patterns of the phased array at different frequencies. Simulated results at (a) 14.4 GHz, (b) 14.8 GHz, and (c) 15.4 GHz and measured results at (d) 14.4 GHz, (e) 14.8 GHz, and (f) 15.4 GHz.
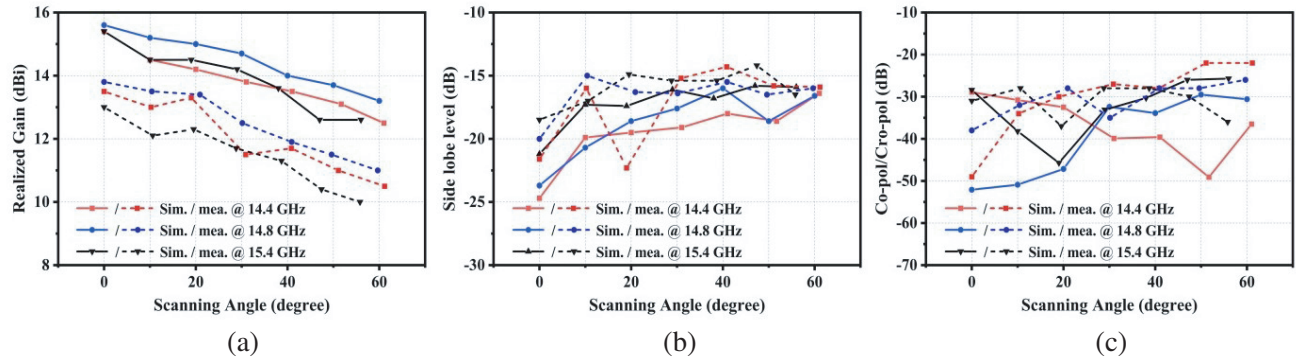

Figure 9. Simulated and measured scanning performance of the proposed 5-bit programmable phased array working at different scanning angles and frequencies. (a) Realized gain, (b) SLL, and (c) cross-polarization.

gains in the broadside direction at the three frequency points are 15.4, 15.6, and 15.4 dBi, respectively, and the corresponding maximum gain fluctuations are 2.9, 2.4, and 2.8 dB, respectively. Meanwhile, the antenna has low SLL and low cross-polarization, which are respectively less than -16 and -30 dB at 14.8 GHz, and less than -15 and -25 dB at low and high frequencies, respectively.

4. FABRICATION AND MEASUREMENT

A sample of the proposed 5-bit programmable phased array antenna was fabricated are shown in Figure 10. In the measurements, each branch was independently controlled by a voltage divider circuit. The S_{11} of the antenna when the scanning angle was $0°$ was measured using an Agilent N5230C vector network analyzer. The measured and simulated results are respectively illustrated by the black and red lines in Figure 11. Clearly, the simulated results agree well with the measured ones.

The radiation properties under different frequencies and scanning angles were measured in a microwave anechoic chamber according to scene and configuration shown in Figures 10(c)–10(d).
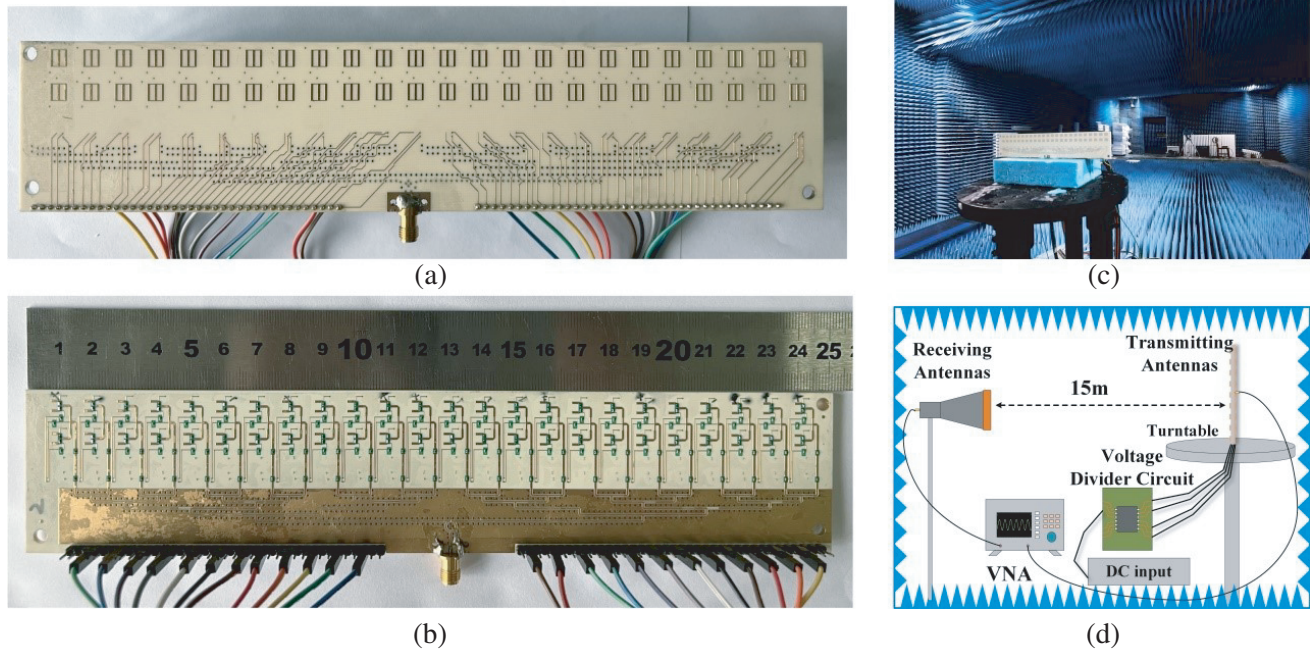
(a)

(c)

(b)

(d)

Figure 10. (a) Top view of the fabricated phased array. (b) Bottom view of the fabricated phased array. (c) Photograph of the measurement scene. (d) Configuration of the measurement.
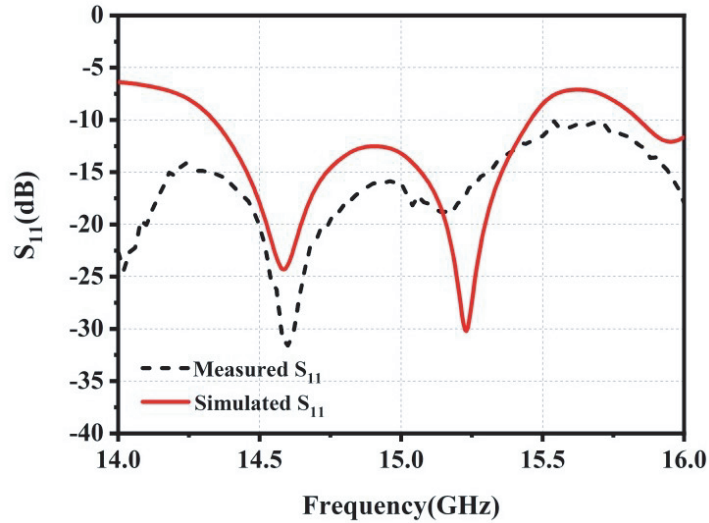

Figure 11. Simulated and measured reflection coefficient results of the proposed phased array when the scanning angle is $0°$.

Because of the spatial symmetry, only the radiation patterns pointing from $0°$ to $60°$ were measured. The results in the H-plane at 14.4, 14.8, and 15.4 GHz are given in Figures 8(d)–8(f), respectively. As can be seen, the beam scanning capability of the phased array is well exhibited in the measurement. In particular, the scanning coverages at the three frequencies are $0°$ to $61°$, $0°$ to $60°$, and $0°$ to $56°$, respectively, consistent with the simulation results. The measured array gain, SLL, and cross-polarization characteristics are summarized in Figure 9. The maximum gains of the antenna in the broadside direction at the three frequencies are 13.5, 13.8, and 13 dBi, respectively, and the maximum gain fluctuations are 3, 2.8, and 3 dB, respectively. The measured gains are a little lower than the

Table 4. Target, simulated and measured scanning angle results at different frequencies.

Freq. (GHz)	Scanning Angles (°)						
14.4	Target	10.4	20.8	30.9	41.2	52.1	62
	Simulated	10	20	31	41	51.7	61
	Measured	10.2	20	30.9	40.8	51	61.2
14.8	Target	10	20.1	30.2	40.3	50.2	60.1
	Simulated	10	20	30	40	50	60
	Measured	10.4	20.9	30.1	40.9	49.6	59.6
15.4	Target	9.7	19.3	29	38.3	47.5	56.4
	Simulated	10	19	29	38	47	56
	Measured	10.6	19.5	28.8	38.7	47.4	55.8

simulated values. This is mainly caused by the intrinsic losses of the dielectric substrates, PIN, and varactor diodes, as well as SMA connectors. Nevertheless, the measured SLL and cross-polarization level at 14.8 GHz are less than -16 and -26 dB at various angles, and those at the low and high frequencies are less than -14 and -22 dB, respectively, which replicate the low SLL and low performance of the simulation. Table 4 summarizes the target, simulated, and measured results. It can be clearly seen that the scanning accuracy of the proposed 5-bit array at different frequencies is less than $1°$. This indicates that the radiation properties of the proposed antenna are stable over the operating band.

Finally, Table 5 compares the performance of the proposed antenna with those previously published in literature. Representative characteristics of reconfigurable array, such as element spacing, polarization, phase quantization bits, diode type and number, operating bandwidth, peak gain, scanning range, SLL, and cross-polarization level are presented. Through the comparison we can find that the proposed antenna realizes higher phase quantization than the previously reported antenna that had rough quantization (1-bit and 2-bit) and even those having the same number of diodes [5, 10, 22, 23]. Hence, the proposed antenna has obvious advantages in terms of scanning accuracy and suppression of SLLs. Moreover, the proposed antenna has wider scanning ranges and lower cross-polarization level than the referenced arrays. The peak gain is actually affected by the element dimension, element spacing, and losses of diodes.

Table 5. Comparison of the proposed design with other referenced antenna arrays.

	This work	[22]	[5]	[23]	[10]
Element Spacing	0.49λ	0.72λ	0.5λ	0.5λ	0.44λ
Polarization	LP	LP	LHCP	LHCP	LP
Phase quantization	5 bit	1 bit	2 bit	2 bit	2 bit
Diode type/number	PIN/2 Varactor/2	PIN/4	PIN/4	PIN/4	PIN/4
Operating Frequency	14.8 GHz	5.7 GHz	3 GHz	3.65 GHz	28 GHz
Bandwidth (%)	6.7	21	1.8	10	7.1
Peak gain (dBi)/ element number	$13.8/24 \times 2$	$19/4 \times 4$	$N.A./8 \times 8$	$11.8/8 \times 1$	$11.7/10 \times 1$
Scanning range	$120°$	$65°$	$86°$	$98°$	$121°$
SLL (dB)	-16	N.A.	-12.5	-7	-5
Cross-polarization (dB)	-26	N.A.	-18	-9	-20

5. CONCLUSION

The design strategy of a low-cost and high-performance 5-bit programmable phased array antenna at Ku-band is presented. By cascading 1-bit reconfigurable radiation elements and a 4-bit reflection-type phase shifter, the proposed phased array can easily achieve 5-bit phase modulation, eliminating the need for numerous electronic phase shifters or T/R components in traditional phased arrays. A 24×2 5-bit programmable phased array antenna operating from 14.4 to 15.4 GHz was designed, fabricated, and measured to verify the design strategy. The results show that the proposed antenna can achieve $0°$–$60°$ high-precision beam scanning with low gain fluctuation, low SLL, and low cross-polarization by controlling the coding sequences in programmable way. The proposed antenna features low cost, low profile, simple fabrication, excellent scanning performance, and convenient programmable control, and contributes to the advances of phased arrays.

APPENDIX A. DESIGN DETAILS OF THE SLOTTED PATCH IN 1-BIT RECONFIGURABLE ANTENNA

Here, we elaborate the advantages of the slotted patch over the conventional rectangular patch in increasing the impedance bandwidth and suppressing cross-polarization. For further illustration, we denote the slotted patch as Ant. 2 and compare it with a simple rectangular patch that is denoted as Ant. 1, as shown in Figures A1(a) and A1(b). Ant. 1 and Ant. 2 have the same parameters except for being not slotted. CST MICROWAVE STUDIO is employed to simulate the two antennas. As shown in Figure A1(c), the impedance bandwidth of Ant. 2 (i.e., the proposed design) was broader than that of Ant. 1, and the impedance matching at high-frequency bands is improved by the slots.
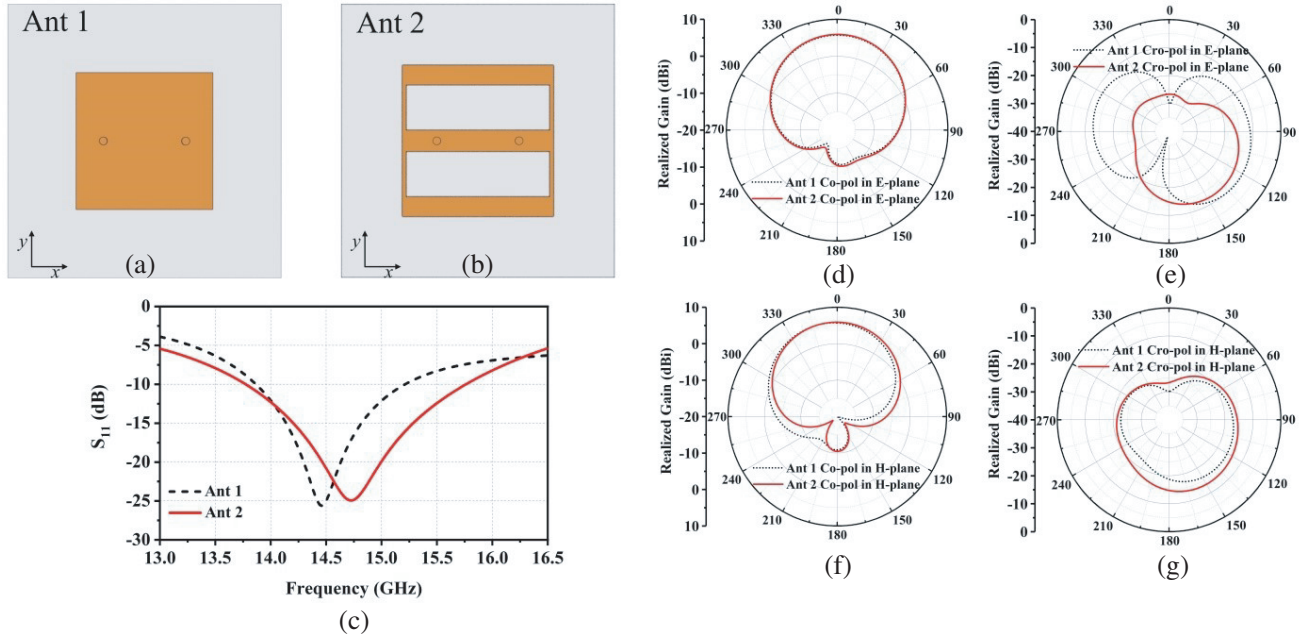

Figure A1. (a) Rectangular patch (Ant. 1). (b) Proposed slotted patch (Ant. 2). (c) Simulated reflection coefficients (S_{11}) of the two patch antennas. (d)–(g) Simulated radiation patterns of the two patch antennas at 14.8 GHz: (d) co-polarization in the E-plane, (e) cross-polarization in the E-plane, (f) co-polarization in the H-plane, and (g) cross-polarization in the H-plane.

The radiation patterns and current distributions of the two antennas at 14.8 GHz are also compared to show the effects of the slots. As shown in Figures A1(d)–A1(g), the co-polarizations of the two antennas in the E-plane and H-plane are basically the same. However, the cross-polarization radiation

of Ant. 2 in the *E*-plane is better than that of Ant. 1. That is to say, low cross-polarization level is obtained through the introduction of the slots. Such a conclusion can also be verified by observing the current distributions of the two antennas shown in Figure A2. As can be seen from Figure A2(a), a certain amount of vertical current is distributed on the rectangular patch, affecting the cross-polarization level of Ant. 1. On the contrary, the slots etched on Ant. 2 cut off the vertical current, hence the current in Figure A2(b) is more uniform than that of Ant. 1. Therefore, the introduced slot enhances the linear
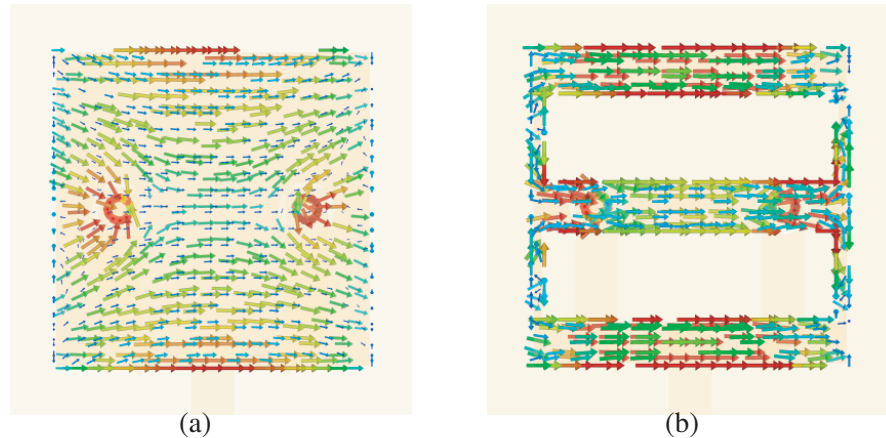

(a)　　　　　　　　　　　　　　　　(b)

Figure A2. Simulated surface current distributions of the two antenna at 14.8 GHz. (a) Ant. 1, (b) Ant. 2.

As mentioned earlier, the slotted patch outperforms the conventional patch in terms of impedance bandwidth and cross-polarization performance, which explains our choice of slotted patches as antenna radiators.

REFERENCES

1. Mailloux, R. J., *Phased Array Antenna Handbook*, 2nd Edition, Artech House, Norwood, MA, USA, 2005.
2. Valavan, S. E., D. Tran, A. G. Yarovoy, and A. G. Roederer, "Dual-band wide-angle scanning planar phased array in X/Ku-bands," *IEEE Trans. Antennas Propag.*, Vol. 62, No. 5, 2514–2521, May 2014.
3. Yang, G., J. Li, R. Xu, Y. Ma, and Y. Qi, "Improving the performance of wide-angle scanning array antenna with a high-impedance periodic structure," *IEEE Antennas Wireless Propag. Lett.*, Vol. 15, 1819–1822, 2016.
4. Beenamole, K. S., P. N. S. Kutiyal, U. K. Revankar, and V. M. Pandharipande, "Resonant microstrip meander line antenna element for wide scan angle active phased array antennas," *Microw. Opt. Technol. Lett.*, Vol. 50, No. 7, 1737–1740, 2008.
5. Yin, L., P. Yang, Y. Gan, F. Yang, S. Yang, and Z. Nie, "A low Cost, low in-Band RCS microstrip phased-array antenna with integrated 2-bit phase shifter," *IEEE Trans. Antennas Propag.*, Vol. 69, No. 8, 4517–4526, Aug. 2021.

6. Li, X., Z. H. Wu, and Q. Cheng, "A 1-Bit reconfigurable antenna in Ku-band," *Proc. Cross Strait Radio Sci. Wirel. Technol. Conf., CSRSWTC1*, 7–9, 2021.

7. Xiao, Y., F. Yang, S. Xu, M. Li, K. Zhu, and H. Sun, "Design and implementation of a wideband 1-Bit transmitarray based on a Yagi–vivaldi unit cell," *IEEE Trans. Antennas Propag.*, Vol. 69, No. 7, 4229–4234, July 2021.

8. Deng, C., D. Liu, B. Yektakhah, and K. Sarabandi, "Series-fed beam-steerable millimeter-wave antenna design with wide spatial coverage for 5G mobile terminals," *IEEE Trans. Antennas Propag.*, Vol. 68, No. 5, 3366–3376, May 2020.

9. Zhang, X. G., W. X. Jiang, H. W. Tian, Z. X. Wang, Q. Wang, and T. J. Cui, "Pattern-reconfigurable planar array antenna characterized by digital coding method," *IEEE Trans. Antennas Propag.*, Vol. 68, No. 2, 1170–1175, February 2020.

10. Wan, X., et al., "Reconfigurable sum and difference beams based on a binary programmable metasurface," *IEEE Antennas and Wireless Propag. Lett.*, Vol. 20, No. 3, 381–385, March 2021.

11. Wang, X. Y., S. C. Tang, and J. X. Chen, "Differential-fed pattern-reconfigurable dielectric patch antenna and array with low cross-polarization," *IEEE Trans. Antennas Propag.*, Vol. 70, No. 5, 3870–3875, 2022.

12. Xiao, S., C. Zheng, M. Li, J. Xiong, and B. Z. Wang, "Varactor-loaded pattern reconfigurable array for wide-angle scanning with low gain fluctuation," *IEEE Trans. Antennas Propag.*, Vol. 63, No. 5, 2364–2369, May 2015.

13. Zhang, Z., S. Cao, and J. Wang, "Azimuth-pattern reconfigurable planar antenna design using characteristic mode analysis," *IEEE Access*, Vol. 9, 60043–60051, 2021.

14. Huang, C., B. Sun, W. B. Pan, and X. G. Luo, "Dynamical beam manipulation based on 2-bit digitally-controlled coding metasurface," *Sci. Rep.*, Vol. 7, 42302, 2017.

15. Dai, J. Y., L. X. Yang, J. C. Ke, et al., "High-efficiency synthesizer for spatial waves based on space-time-coding digital metasurface," *Laser & Photonics Reviews*, Vol. 14, 1900133, 2020.

16. Wang, Q., et al., "Millimeter-wave digital coding metasurfaces based on nematic liquid crystals," *Adv. Theory Simul.*, Vol. 2, No. 12, Art. No. 1900141, 2019.

17. Yi, D., X. Wei, and Y. Xu, "Tunable microwave absorber based on patterned graphene," *IEEE Trans. Microw. Theory Tech.*, Vol. 65, No. 8, 2819–2826, August 2017.

18. Cui, T. J., M. Q. Qi, X. Wan, J. Zhao, and Q. Cheng, "Coding metamaterials, digital metamaterials and programmable metamaterials," *Light-Sci. Appl.*, Vol. 3, No. 10, 218, October 2014.

19. Yang, H., et al., "A 1-bit 10×10 reconfigurable reflectarray antenna: Design, optimization, and experiment," *IEEE Trans. Antennas Propag.*, Vol. 64, No. 6, 2246–2254, June 2016.

20. Wang, Y., S. H. Xu, F. Yang, and D. H. Werner, "1 bit dual-linear polarized reconfigurable transmitarray antenna using asymmetric dipole elements with parasitic bypass dipoles," *IEEE Trans. Antenna Propag.*, Vol. 69, No. 2, 1188–1192, February 2021.

21. Yang, J., et al., "Folded transmitarray antenna with circular polarization based on metasurface," *IEEE Trans. Antenna Propag.*, Vol. 69, No. 2, 806–814, February 2021.

22. Hu, J., Z. Hao, and Y. Wang, "A wideband array antenna with 1-bit digital-controllable radiation beams," *IEEE Access*, Vol. 6, 10858–10866, 2018.

23. Liu, P., Y. Li, and Z. Zhang, "Circularly polarized 2 Bit reconfigurable beam-steering antenna array," *IEEE Trans. Antenna Propag.*, Vol. 68, No. 3, 2416–2421, March 2020.

24. CST MWS, Accessed: 2020, [Online], Available: https://www.cst.com/products/cstmws.

25. Henoch, B. T. and P. Tamm, "A 360 reflection-type diode phase modulator," *IEEE Trans. Microw. Theory Tech.*, Vol. 19, No. 1, 103–105, January 1971.

26. Hardin, R. N., E. J. Downey, and J. Munushian, "Electronically variable phase shifter utilizing variable capacitance diodes," *Proc. IRE*, Vol. 48, No. 5, 944–945, May 1960.

27. Lin, C., S. Chang, C. Chang, and Y. Shu, "Design of a reflection-type phase shifter with wide relative phase shift and constant insertion loss," *IEEE Trans. Microw. Theory Tech.*, Vol. 55, No. 9, 1862–1868, September 2007.

28. Ellinger, F., R. Vogt, and W. Bachtold, "Compact reflective-type phase-shifter MMIC for C-band using a lumped-element coupler," *IEEE Trans. Microw. Theory Tech.*, Vol. 49, No. 5, 913–917, May 2001.

29. Gupta, R. K., S. E. Anderson, and W. J. Getsinger, "Impedance-transforming 3-dB 90° hybrids," *IEEE Trans. Microw. Theory Tech.*, Vol. 35, No. 12, 1303–1307, December 1987.

30. Pozar, D. M., *Microwave Engineering*, Wiley, Hoboken, NJ, USA, 2009.